Cirrus Radiative Properties in the Tropical Western Pacific

J. M. Comstock and T. P. Ackerman
Pacific Northwest National Laboratory
Richland, Washington

G. G. Mace
University of Utah
Salt Lake City, Utah

Introduction

Cirrus clouds in tropical regions are often located high in the cold upper troposphere and have low optical depths. In addition, tropical cirrus often extend in large sheets up to 1000 km horizontally, which may have a large influence on the energy budget of the atmosphere. Characterizing the location and radiative properties of cirrus clouds is an important step in understanding the processes that generate and maintain these cold, thin cirrus clouds and their impact on upper tropospheric dynamics.

In this paper, we present cirrus radiative properties derived using a combination of Micropulse Lidar (MPL) and Atmospheric Emitted Radiance Interferometer (AERI) measurements obtained at the Atmospheric Radiation Measurement (ARM) Tropical Western Pacific (TWP) site located on Nauru Island. Results are compiled for April through December 1999 and are compared with microphysical retrievals from Millimeter-Wave Cloud Radar (MMCR) measurements.

The main points addressed in this paper are first to compare the heights and visible optical depths of tropical cirrus derived independently from lidar and radar retrieval techniques. Second, we examine the differences in radiative heating rates for several cirrus clouds observed in the TWP region. Mechanisms that are important in the formation and persistence of tropical cirrus are also discussed to help assess the impact of these high, cold, thin cirrus on the radiation balance in the tropics.

Lidar Retrieval Algorithm

Cloud visible optical depth τ and infrared (IR) emittance ε are derived by combining MPL and AERI measurements in an iterative technique that relates IR absorption in cirrus clouds to the visible extinction coefficient. This algorithm is based on the lidar/radiometer (LIRAD) method of Platt and Dilley (1981) with modifications described in Comstock and Sassen (2001).

The MPL located on Nauru emits a 10 to 15 μJ pulse at a wavelength of 532 nm with a pulse repetition frequency (PRF) of 2500 Hz. The vertical resolution is 30 m and the receiver field-of-view (FOV) is 100 μm, which helps to minimize the effects of forward multiple scattering on the retrieved optical depth.

The AERI instrument measures the absolute IR spectral radiance of the atmospheric column above the instrument and spectrally scans between 500 and 3300 wavenumbers (cm^{-1}) at a 1.0 cm^{-1} resolution. AERI radiance measurements used in the calculation of ε are integrated between 833 cm^{-1} and 1081 cm^{-1}.

Visible optical depth τ (532 nm) is calculated using the cloud backscatter coefficient β_c integrated between cloud base z_b and top z_t heights:

$$\tau = \tfrac{1}{k} \int_{z_b}^{z_t} \beta_c(z) dz \,,$$

where k is the backscatter-to-extinction ratio. The parameter k is estimated by first calculating the average backscatter coefficient $\overline{\beta}$ between cloud top and the maximum height of the lidar signal for many values of k between 0.01 and 0.2. We then numerically determine where the change in $\overline{\beta}$ becomes small as k changes. The parameter β_c is assumed to be related to the IR absorption coefficient σ_a and an iterative calculation is performed until the AERI-measured and model-calculated cloud radiances agree. Cloud emittance is related to σ_a using

$$\varepsilon = 1 - \exp\left(-\int_{z_b}^{z_t} \sigma_a(z) dz \right).$$

Radar Retrieval Algorithm

Results of τ and ε are also derived using a combination of MMCR and AERI (800 to 1000 cm^{-1}) measurements. The MMCR operates at 34.86 GHz with ~90 m range resolution up to 15.045 km. The retrieval algorithm described in Mace et al. (1998) produces estimates of τ, ε, ice water content (IWC), and effective radius re. Using an initial guess of ε, an equation relating ε, cloud thickness Δz, radar reflectivity, and modal diameter is numerically solved to determine ice water path (IWP) and particle size. A modified gamma particle size distribution is assumed for the retrieval.

The radiative parameterizations of Fu and Liou (1993) and the MODTRAN (Berk et al. 1989) radiative transfer algorithm are used to estimate downwelling radiance. The computed radiance is then compared to the measured AERI radiance for specific spectral bands. This process is repeated by adjusting ε until the measured and modeled radiances are in agreement. Visible optical depth (0.55 μm) is then calculated by inserting the retrieved re and IWP into Fu and Liou (1993) parameterizations.

Comparisons of Cloud Height and Visible Optical Depth

Comparisons of cloud base and top height detected by the MPL and MMCR are displayed in Figure 1. Probability distribution functions (PDFs) of z_t and z_b reveal distinct differences between each remote sensor. Because of dynamic range limitations, the radar does not detect clouds above 15 km, which is clearly depicted in Figure 1a where ~34% of lidar observations of cirrus have z_t > 15 km. Approximately 8% of lidar cloud base observations lie above 15 km (Figure 1b), and these clouds have an

average $\tau \sim 0.086$. Results for z_t in Figure 1a are consistent with observations from airborne lidar measurements obtained during the Tropical Ocean Global Atmosphere-Coupled Ocean Atmosphere Response Experiment (TOGA/COARE) (Sassen et al. 2000).
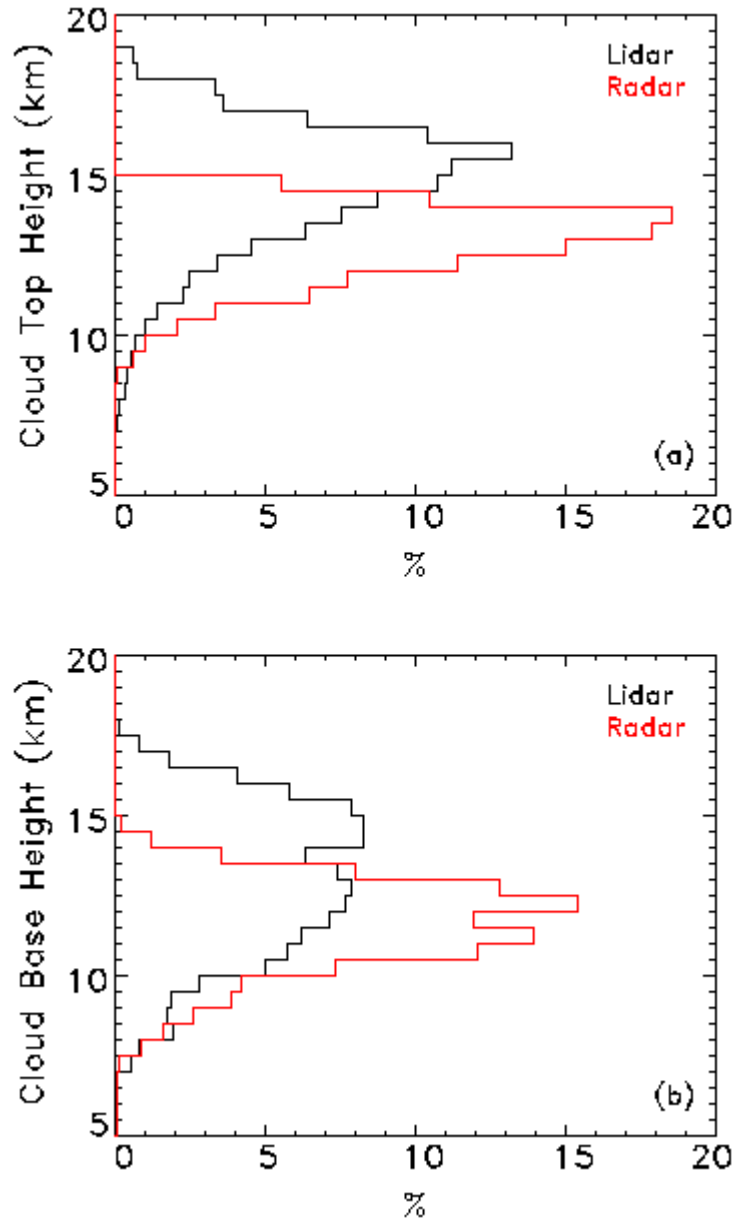

Figure 1. Frequency of occurrence (%) of (a) cirrus cloud top and (b) cloud base height detected by lidar and radar over Nauru Island between April and December 1999.

Figure 2 compares PDFs of lidar- and radar-derived visible optical depth. The apparent uniformity in the two PDFs is displayed in Figure 2a, where τ extends between 0 and 2. Figure 2a also shows the upper limit of MPL observations in thicker cirrus clouds. Lidar signals become attenuation-limited in optically thick clouds usually as τ approaches 3. Due to its low output energy, the MPL tends to become fully attenuated as τ approaches 2. Radar-derived $\tau > 1.0$ consists of 8% of the measurements, as compared with only 4% of lidar results.
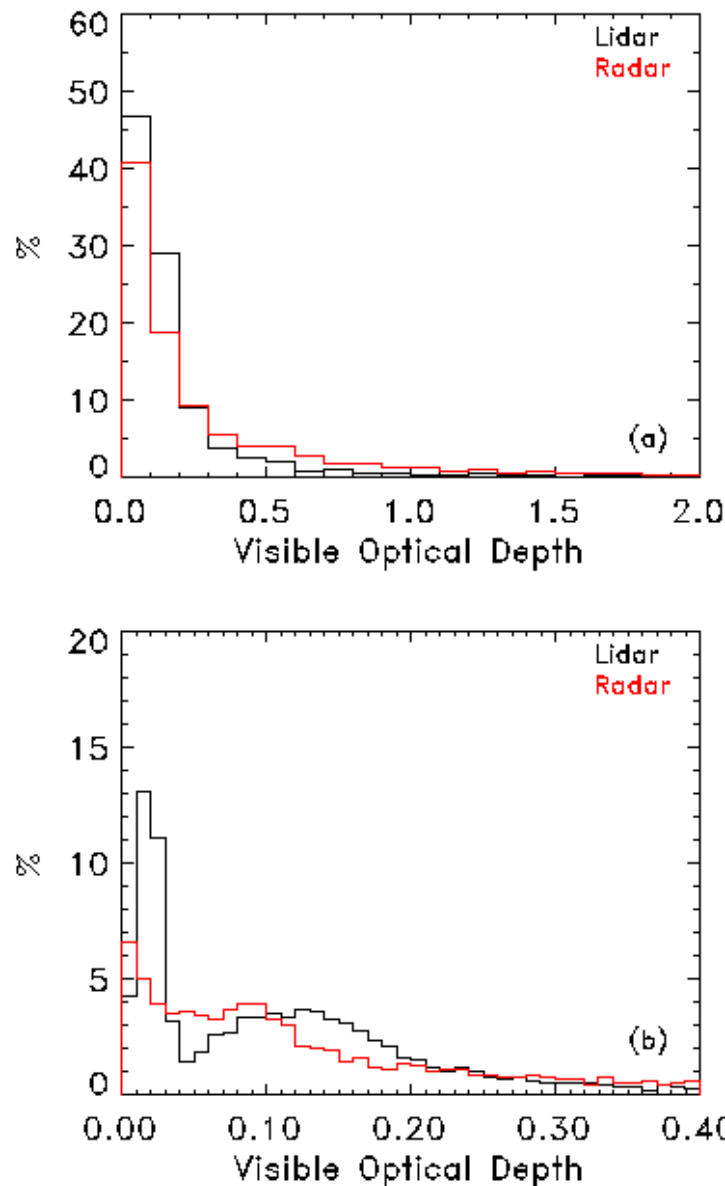

Figure 2. Frequency of occurrence (%) of cirrus visible optical depth estimated using lidar and radar retrieval methods for the same time period as in Figure 1. (a) τ between 0.0 and 2.0, and (b) for τ between 0.0 and 0.4.

Agreement between the two instruments is not as good for small optical depths. There is a striking peak in lidar derived τ at ~0.015 (Figure 2b), which is less than the maximum threshold for subvisual cirrus ($\tau < 0.03$; Sassen and Cho 1992). Since the strong peak does not appear in the radar results, we can infer that this cirrus may correspond to observations with $z_b > 15$ km.

Cirrus Cloud Formation and Persistence Mechanisms

Several mechanisms have been identified as possible contributors to the formation and persistence of tropical cirrus. The two most general formation mechanisms are (1) cirrus due to anvil outflows of cumulonimbus clouds, and (2) as a result of synoptic scale uplift (Jensen et al. 1996). More recently, several specific mechanisms have been examined. For example, Boehm and Verlinde (2000) link tropopause "trap" cirrus, found almost exclusively in the tropics, with large-scale variability near the tropopause and downward phase propagation of Kelvin waves from the lower stratosphere. Cirrus occurrence is also linked to cold temperature perturbations in the upper troposphere. Hartmann et al. (2001) hypothesize that subvisual cirrus located above thicker anvil clouds persist due to radiative cooling in the upper layer that is caused by the underlying anvil.

To link the mechanisms described above with actual observations of cirrus clouds, MPL measurements from Nauru are divided into categories based on height and cloud layers (Figure 3). The categories include single layer high cirrus ($z_b > 12$ km), single layer low ($z_b < 12$ km), and multiple layered clouds with varying distances between layers. Approximately 36% of lidar observations have a single layer and are high in the troposphere and ~47% have multiple layers. Single/low clouds consist of ~18% of the observations; however, if the lidar signal is fully attenuated, layers aloft will not be detected.
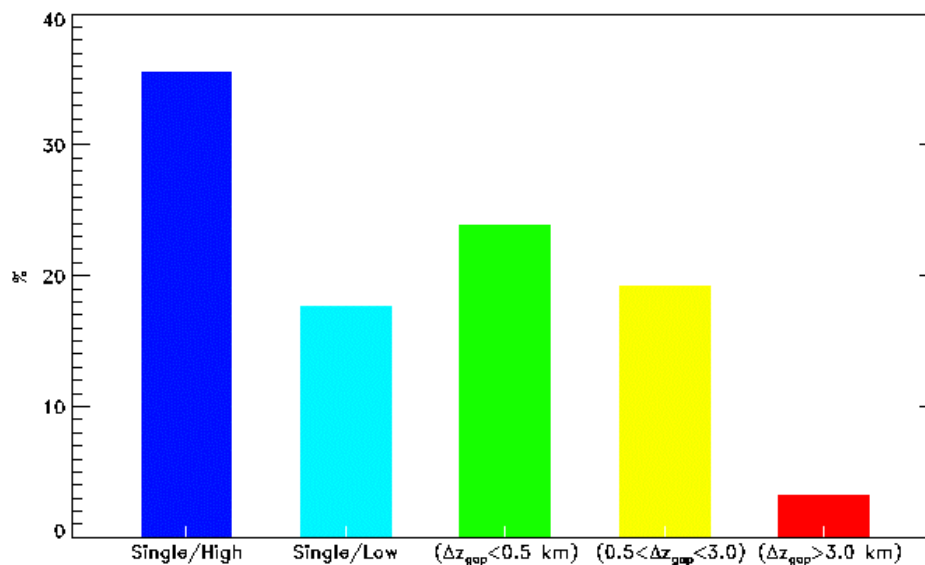

Figure 3. Cirrus cloud occurrence (%) divided according to cloud height and number of layers. The symbol Δz_{gap} indicates the distance (km) between layers. Observations are derived from MPL measurements between April and December 1999 at Nauru Island.

Tropical Cirrus Cases Observed over Nauru Island

Using the above cirrus cloud types as a guide, we identify four cases that represent "typical" cirrus observations over Nauru Island to help examine the radiative impact of high clouds on the radiation balance in the tropics. Heating rate calculations are made for each case using the following technique. First, lidar-derived τ and Δz are averaged over a 1-hr to 2-hr period when there is uniform cloud base and top heights and a relatively constant τ. Mean layer extinction coefficient $\overline{\sigma}_e$ is estimated from mean τ and Δz. Using the lidar backscatter profile averaged over the same time period as a weighting function, $\overline{\sigma}_e$ is distributed throughout the cloud layer. Assuming a generalized effective size D_{ge}, IWC is determined following the parameterization from Fu (1996). Fluxes and heating rates are calculated by inserting atmospheric thermodynamic profiles from the nearest radiosonde launch time from Nauru Island using the correlated K distribution model and δ-4 stream radiative transfer code described in Fu and Liou (1992, 1993).

The first example (Figure 4) is a single layer subvisual cirrus located at ~15 km. As displayed in the time vs. height image of MPL backscattered energy (Figure 4d), the cirrus cloud persists for over 18 hr with no underlying clouds. The MMCR is unable to detect cirrus on this day. Average MPL derived τ is ~0.028 for the time period between 1300 Universal Time Coordinates (UTC) and 1500 UTC. Although the cirrus layer is subvisual, there is noticeable IR heating in the upper troposphere due to the presence of the cloud (Figure 4c).

An example of a low, thick, single-layer cirrus is illustrated in Figure 5. Comparisons of radar-and lidar-derived cloud height, τ, and ε show good agreement for this case. In some instances, the attenuation limiting behavior of the lidar is visible (Figure 5e), which is apparent in the higher cloud top detected by the radar. This optically thick cloud has an average $\tau \sim 0.667$ during 0900 UTC and 1000 UTC, which results in net heating in the cloud layer that is on the same order as the subvisual layer in Figure 4. However, in this case, the heating is mainly due to solar heating.

Both optically thick and thin clouds occur in multiple layers. Figure 6 displays a subvisual layer above an optically thin cloud that has an average total $\tau \sim 0.14$ between 1730 UTC and 1830 UTC. As shown in Figure 5, there is good agreement between lidar- and radar-derived radiative properties during the time periods where the cloud is detected by each instrument. Net heating in the upper layer is nearly the same as the thicker lower layer and the maximum heating rate is higher than in either of the single-layer cases.

Lastly, Figure 7 exhibits a multi-layer example where the lower layer is optically thick ($\tau \sim 1.8$), the upper layer is subvisual ($\tau \sim 0.024$), and there is a substantial gap between layers (3.3 km). Net heating rates (Figure 7c) indicate cloud top cooling in the lower layer and virtually no heating in the upper layer. Figure 7a does display slight solar heating caused by the upper layer.
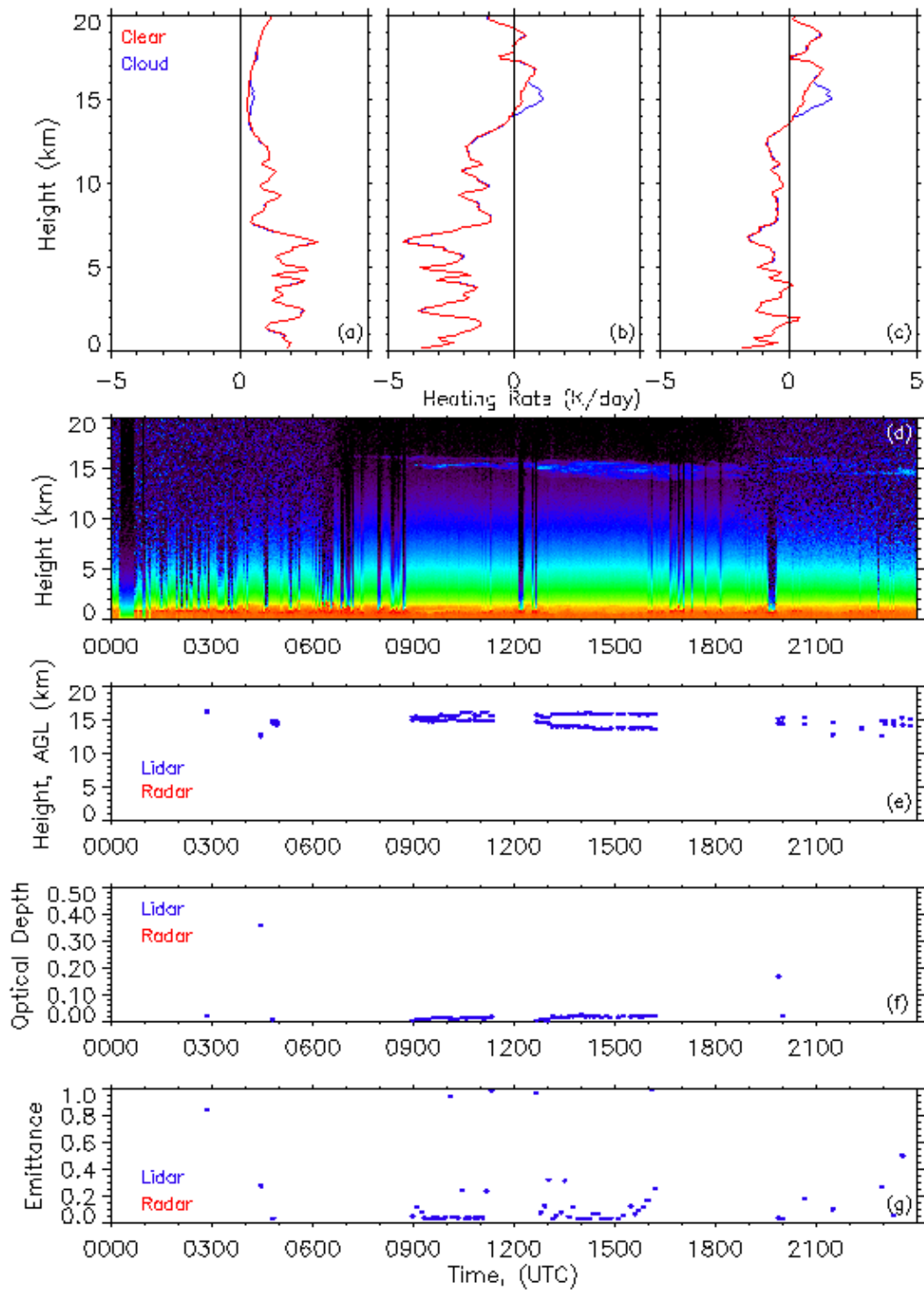
Figure 4. Radiative properties and heating rates derived using MPL and AERI measurements for a cirrus cloud observed on October 25, 1999, at Nauru Island: (a) solar, (b) IR, and (c) net heating rates (K/day). (d) Time vs. height display of lidar normalized backscattered energy, (e) cloud boundaries, (f) visible optical depth, and (g) cloud IR emittance.
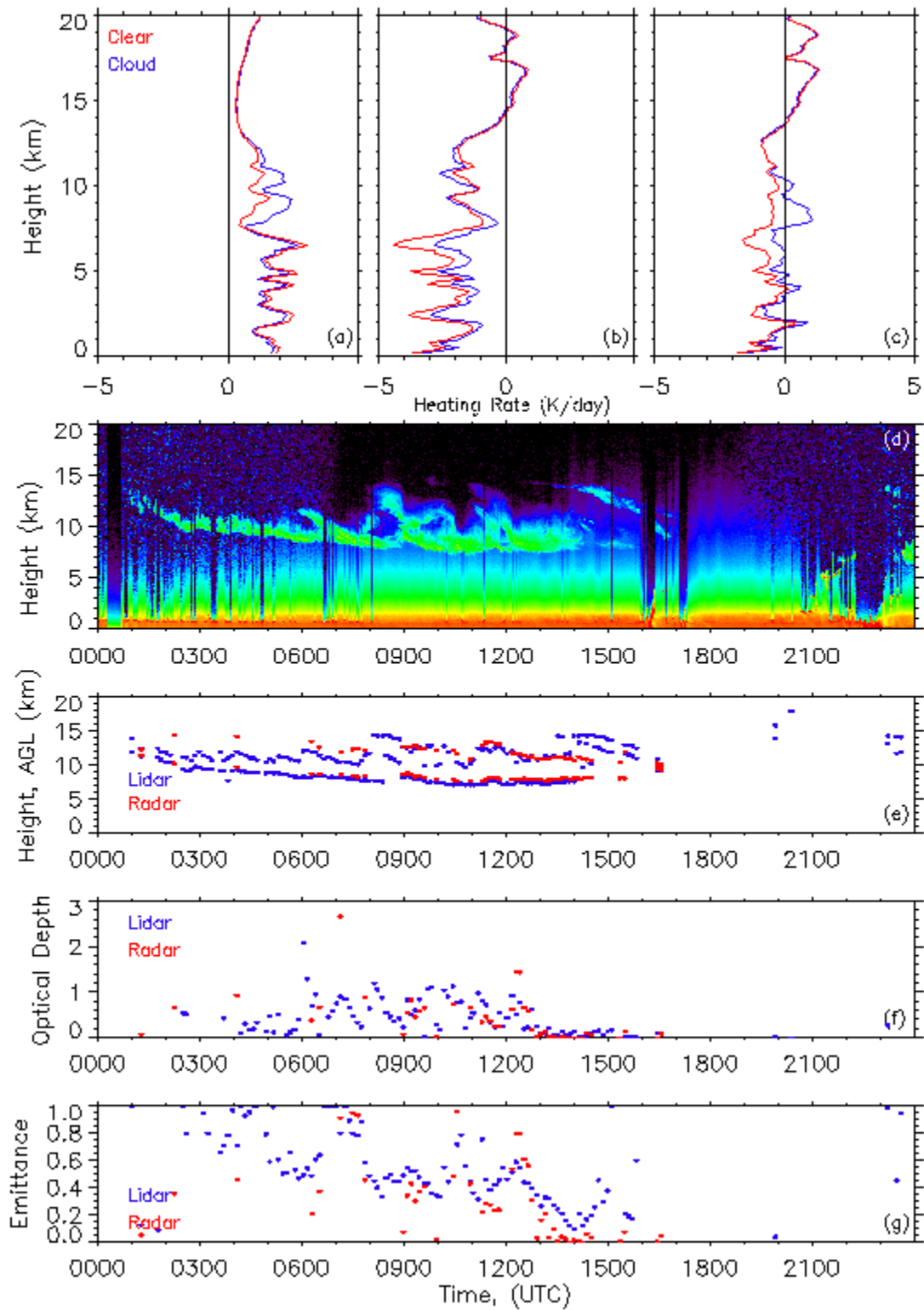
Figure 5. Same as in Figure 4, except for cirrus observed on July 7, 1999. Also shown are radar-derived radiative properties and cloud boundaries.
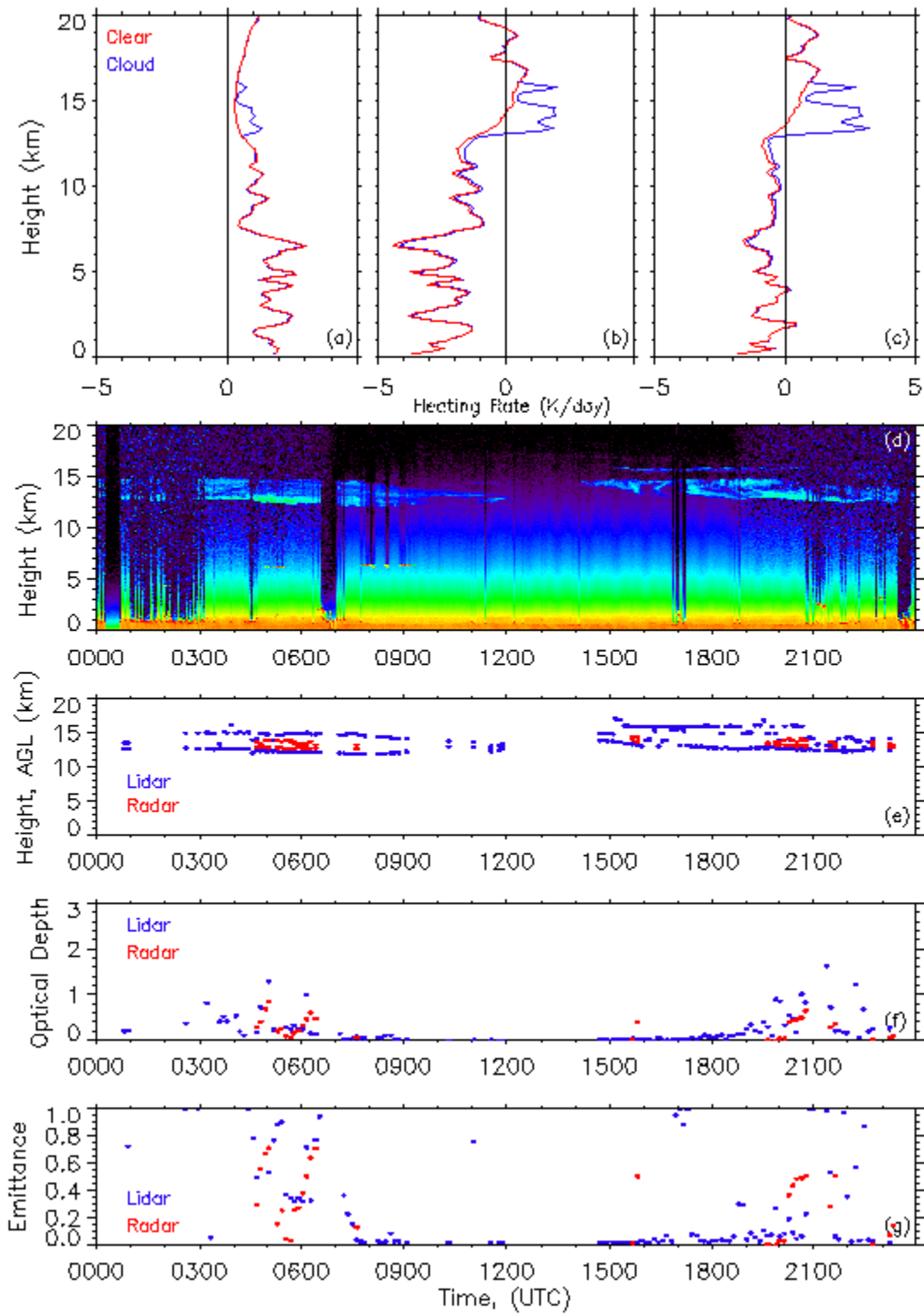
Figure 6. Same as in Figures 4 and 5, except for cirrus observed on July 10, 1999.
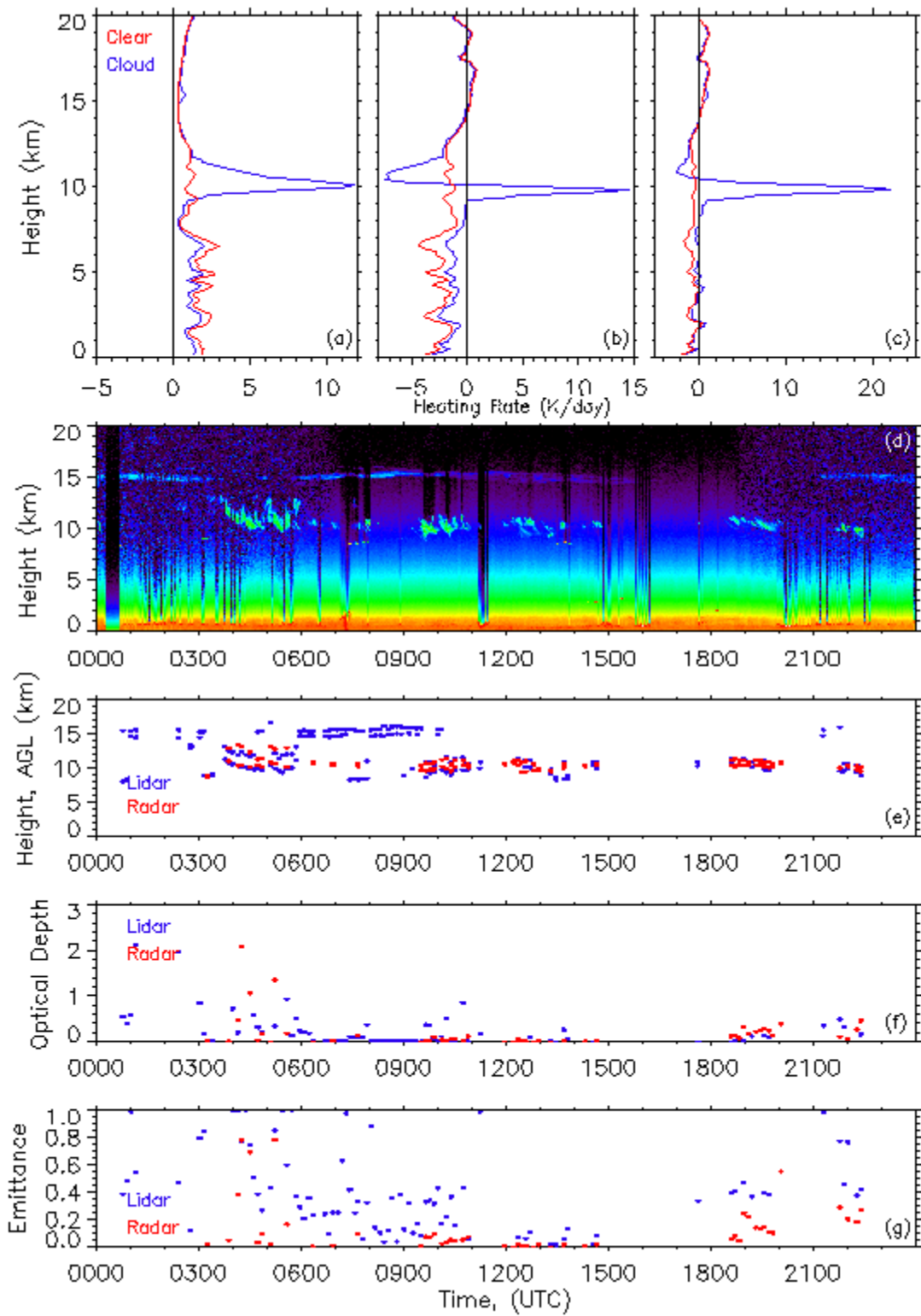
Figure 7. Same as in Figures 4 and 5, except for cirrus observed on June 18, 1999.

Discussion

From these observations of tropical cirrus, we conclude that, using independent ground-based active remote sensors, we can obtain fairly good agreement in derived radiative properties. Although each retrieval has weaknesses, together the complementary instruments help achieve a better understanding of the radiative and microphysical properties of cirrus clouds.

In this study, we have also presented heating rates calculated using ground-based remotely sensed radiative properties for four examples of tropical cirrus. Our results indicate that heating rates vary significantly for different cirrus types. Each cirrus type can be linked to a mechanism that is responsible for the formation of cloud layers. However, verification of remotely sensed cloud microphysical properties and model heating rates are important to accurately study the dynamic processes associated with the formation and maintenance of tropical cirrus.

Corresponding Author

J. M. Comstock, Jennifer.Comstock@pnl.gov, 509-372-4244

References

Berk, A., L. S. Bernstein, and D. C. Robertson, 1989: MODTRAN: A moderate resolution model for LOWTRAN7, Tech. Rep. GL-TR-89-0122, 38 pp. Available from Geophys. Lab., Hanscom Air Force Base, Massachusetts.

Boehm, M. T., and J. Verlinde, 2000: Stratospheric influence on upper tropospheric tropical cirrus. *Geophys. Res. Let*., **27**, 3209-3212.

Comstock, J. M., and K. Sassen, 2001: Retrieval of cirrus cloud radiative and backscattering properties using combined lidar and infrared radiometer (LIRAD) measurements. *J. Oceanic and Atmos. Tech*. Accepted.

Fu, Q., 1996: An accurate parameterization of the solar radiative properties of cirrus clouds for climate models. *J. of Climate*, **9**, 2058-2082.

Fu, Q., and K. N. Liou, 1992: On the correlated k-distribution method for radiative transfer in nonhomogeneous atmospheres. *J. Atmos. Sci*., **49**, 2139-2156.

Fu, Q., and K. N. Liou, 1993: Parameterization of the radiative properties of cirrus clouds. *J. Atmos. Sci*., **50**, 2008-2025.

Hartmann, D. L., J. R. Holton, and Q. Fu, 2001: The heat balance of the tropical tropopause, cirrus, and stratospheric dehydration. *Geophys. Res. Let.* Accepted.

Jensen, E. J., O. B. Toon, H. B. Selkirk, J. D. Spinhirne, and M. R. Schoeberl, 1996: On the formation and persistence of subvisible cirrus clouds near the tropical tropopause. *J. Geophys. Res*., **101**, 21,361-21,375.

Mace, G. G., T. P. Ackerman, P. Minnis, and D. F. Young, 1998: Cirrus layer microphysical properties derived from surface-based millimeter radar and infrared interferometer data. *J. Geophys. Res*., **103**, 23,207-23,216.

Platt, C.M.R., and A. C. Dilley, 1981: Remote sensing of high clouds. Part IV, Observed temperature variations in cirrus optical profiles. *J. Atmos. Sci.*, **38**, 1069-1082.

Sassen, K., and B. S. Cho, 1992: Subvisual-thin cirrus lidar dataset for satellite verification and climatological research. *J. Appl. Met*., **31**, 1275-1285.

Sassen, K., R. P. Benson, and J. D. Spinhirne, 2000: Tropical cirrus cloud properties derived from TOGA/COARE airborne polarization lidar. *Geophys. Res. Let*., **27**, 673-676.